

Chemical Science

rsc.li/chemical-science



ISSN 2041-6539



ROYAL SOCIETY
OF CHEMISTRY

EDGE ARTICLE

Yousung Jung, Zhenyu Sun *et al.*

Carbon-supported Ni nanoparticles for efficient CO₂ electroreduction

Cite this: *Chem. Sci.*, 2018, 9, 8775

All publication charges for this article have been paid for by the Royal Society of Chemistry

Carbon-supported Ni nanoparticles for efficient CO₂ electroreduction†

Mingwen Jia,^a Changhyeok Choi,^b Tai-Sing Wu,^c Chen Ma,^d Peng Kang,^e Hengcong Tao,^a Qun Fan,^a Song Hong,^a Shizhen Liu,^a Yun-Liang Soo,^c Yousung Jung,^b Jieshan Qiu^a and Zhenyu Sun^{*,a}

The development of highly selective, low cost, and energy-efficient electrocatalysts is crucial for CO₂ electrocatalysis to mitigate energy shortages and to lower the global carbon footprint. Herein, we first report that carbon-coated Ni nanoparticles supported on N-doped carbon enable efficient electroreduction of CO₂ to CO. In contrast to most previously reported Ni metal catalysts that resulted in severe hydrogen evolution during CO₂ conversion, the Ni particle catalyst here presents an unprecedented CO faradaic efficiency of approximately 94% at an overpotential of 0.59 V, even comparable to that of the best single Ni sites. The catalyst also affords a high CO partial current density and a large CO turnover frequency, reaching 22.7 mA cm⁻² and 697 h⁻¹ at -1.1 V (versus the reversible hydrogen electrode), respectively. Experiments combined with density functional theory calculations showed that the carbon layer coated on Ni and N-dopants in carbon material both play important roles in improving catalytic activity for electrochemical CO₂ reduction to CO by stabilizing *COOH without affecting the easy *CO desorption ability of the catalyst.

Received 21st August 2018
Accepted 4th November 2018

DOI: 10.1039/c8sc03732a

rsc.li/chemical-science

Introduction

Direct electrochemical reduction of CO₂ (ECR) powered by electricity from renewable sources provides a “clean” and efficient way to alleviate the greenhouse effect and to convert CO₂ into value-added fuels and chemicals.^{1–10} Despite the recent progress made in ECR,^{11–16} it still suffers from (1) a large overpotential, (2) sluggish electron transfer kinetics, (3) insufficient product selectivity, and (4) degradation of catalytic activity within short periods. Additionally, proton reduction to generate H₂ always takes place as a competitive reaction, especially in aqueous solutions, which lowers CO₂ reduction selectivity and efficiency. Extensive efforts are therefore being devoted to developing new electrocatalysts that can reduce CO₂ at high

rates with low overpotentials and large turnover frequencies (TOFs).

The reduction of CO₂ to CO [CO₂ + 2H⁺ + 2e⁻ → CO + H₂O, E_{redox}⁰ = -0.11 V vs. the reversible hydrogen electrode (RHE)] proceeds through a two-electron (e⁻)/proton (H⁺) transfer pathway.⁷ A CO₂ molecule is first reduced to a carboxyl intermediate (*COOH) either by a concerted e⁻/H⁺ or by a decoupled e⁻ and H⁺ transfer that involves the formation of a CO₂⁻ radical. Subsequently, a second e⁻/H⁺ attacks the oxygen atom (OH) in the *COOH to generate H₂O (l) and CO. Au,¹⁷ Ag,¹⁷ modified Pd,^{18,19} and bimetallic Cu²⁰ can tightly bind *COOH, which is further reduced to a *CO intermediate in aqueous media. The *CO is weakly bound to their surfaces, and CO desorbs from the metal electrodes as a major product. Despite their high CO₂-to-CO conversion, the high cost and scarcity of these metals are problematic for practical applications. Exploration of cheap and earth-abundant catalysts for efficient CO₂ electrocatalysis is thus desirable. Late transition metals such as Fe, Co, and Ni are promising alternatives to expensive noble metals. However, metallic Fe, Co, and Ni tend to promote the hydrogen evolution reaction (HER). They also possess strong bonding with adsorbed CO, dramatically limiting ECR. To solve this problem, construction of single metal sites has been demonstrated to enable engineering of the electronic properties of transition metals for enhanced ECR.^{21–26} It was speculated that charge transfer occurred between the metal atoms with delocalized electrons and the carbon 2p orbital in CO₂ to form a CO₂^{δ-} species, thereby reducing the energy barrier for ECR.

^aState Key Laboratory of Organic-Inorganic Composites, College of Chemical Engineering, Beijing University of Chemical Technology, Beijing 100029, P. R. China. E-mail: sunzy@mail.buct.edu.cn

^bGraduate School of EEWS, Korea Advanced Institute of Science and Technology (KAIST), Daejeon 34141, Republic of Korea. E-mail: ysjn@kaist.ac.kr

^cDepartment of Physics, National Tsing Hua University, Hsinchu, Taiwan 30013

^dTechnical Institute of Physics and Chemistry, Chinese Academy of Sciences, Beijing 100190, P. R. China

^eSchool of Chemical Engineering and Technology, Tianjin University, Tianjin 300072, P. R. China

† Electronic supplementary information (ESI) available: Experimental details, TEM and HRTEM images, XPS survey, linear sweep voltammetry, cyclic voltammograms, Faradaic efficiency, and DFT calculation details. See DOI: 10.1039/c8sc03732a



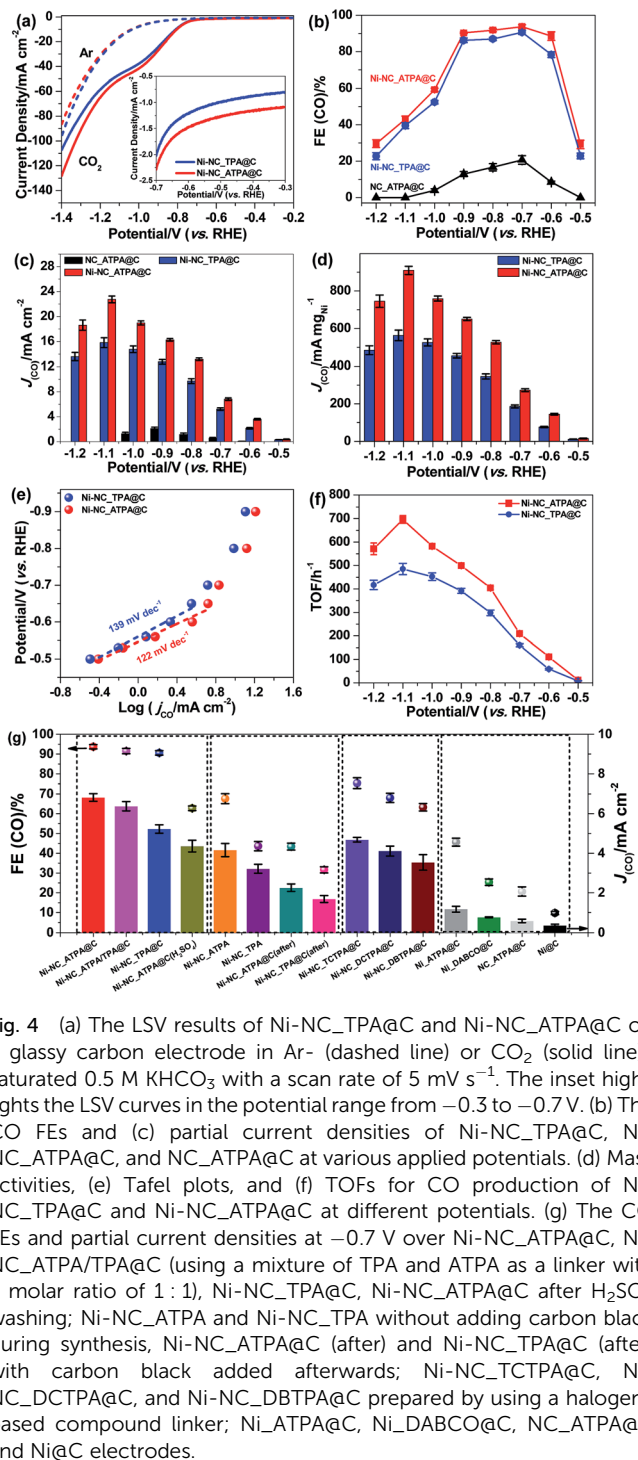


Fig. 4 (a) The LSV results of Ni-NC_TPA@C and Ni-NC_ATPA@C on a glassy carbon electrode in Ar- (dashed line) or CO₂ (solid line)-saturated 0.5 M KHCO₃ with a scan rate of 5 mV s⁻¹. The inset highlights the LSV curves in the potential range from -0.3 to -0.7 V. (b) The CO FEs and (c) partial current densities of Ni-NC_TPA@C, Ni-NC_ATPA@C, and NC_ATPA@C at various applied potentials. (d) Mass activities, (e) Tafel plots, and (f) TOFs for CO production of Ni-NC_TPA@C and Ni-NC_ATPA@C at different potentials. (g) The CO FEs and partial current densities at -0.7 V over Ni-NC_ATPA@C, Ni-NC_ATPA/TPA@C (using a mixture of TPA and ATPA as a linker with a molar ratio of 1 : 1), Ni-NC_TPA@C, Ni-NC_ATPA@C after H₂SO₄ washing; Ni-NC_ATPA and Ni-NC_TPA without adding carbon black during synthesis, Ni-NC_ATPA@C (after) and Ni-NC_TPA@C (after) with carbon black added afterwards; Ni-NC_TCTPA@C, Ni-NC_DCTPA@C, and Ni-NC_DBTPA@C prepared by using a halogen-based compound linker; Ni_ATPA@C, Ni_DABCO@C, NC_ATPA@C and Ni@C electrodes.

catalysts determines the reaction rate. But Ni-NC_ATPA@C has faster kinetics for CO₂ reduction than Ni-NC_TPA@C. Likewise, Ni-NC_ATPA@C exhibited larger CO formation TOFs than Ni-NC_TPA@C (Fig. 4f and S4†), and achieved 697 h⁻¹ at -1.1 V based on electrochemical surface area determination from double layer capacitance measurements. The Ni-NC_ATPA@C catalyst retained a stable current density over 6 mA cm⁻² and a CO FE of about 93% after electrolysis for 24 h at -0.7 V (Fig. S5†).

In order to probe the active centers in carbon supported Ni catalysts, control experiments were performed on different Ni catalysts that were produced with varying linkers, as displayed in Fig. 4g. It was found that N doped carbon in the absence of Ni (NC_ATPA@C) showed very low ECR activity toward CO generation (Fig. 4b, c, and g, and S3†), suggesting that Ni is responsible for efficient ECR. Nevertheless, Ni particles supported on carbon black without nitrogen modification (Ni@C) also exhibited poor ECR activity. This indicates that N doping plays an important role in facilitating CO₂-to-CO conversion. The ECR performance in terms of both CO FE and partial current density increased with N content. This can be evidenced by the significantly lower activity of the two Ni catalysts prepared by using only ATPA (Ni_ATPA@C) or DABCO (Ni_DABCO@C) without addition of another organic linker, which have lower N content as compared with Ni-NC_TPA@C, Ni-NC_TPA/ATPA@C, and Ni-NC_ATPA@C. We also made efforts to modify the carbon support with N and halogen (Cl or Br) atoms by using DCTPA, DBTPA, or TCTPA as a linker. However, the resultant Ni catalysts supported on N, Cl or Br co-doped carbon did not show improved ECR activity compared with Ni-NC_TPA@C. The Ni-NC_TPA and Ni-NC_ATPA without incorporation of carbon black, and Ni-NC_TPA@C (after) and Ni-NC_ATPA@C (after) with equivalent amounts of carbon black mixed afterwards all have lower CO FEs and partial current densities relative to the corresponding Ni catalysts with addition of carbon black during the preparation process. The pyrolysis temperature was observed to considerably influence the ECR performance of the catalyst as well, with 800 °C likely being the optimal reaction temperature (Fig. S6†). Furthermore, we found that acid treatment of Ni-NC_ATPA@C in 2 M H₂SO₄ for 1 h led to a pronounced decrease of the CO FE from ~93.7% to ~62.7%, highlighting that Ni NPs contribute to the ECR (Fig. 4g).

To investigate the effects of carbon coating on Ni nanoparticles and nitrogen content in carbon supports on the catalytic activity and selectivity of ECR, we performed DFT calculations. We considered a graphene (Gr) monolayer on a Ni(111) surface (Gr/Ni(111)) to model the carbon coating on Ni nanoparticles. Previous studies on graphene on Ni(111) by using high-resolution X-ray photoelectron spectroscopy (HR-XPS) combined with DFT calculations showed that the two different graphene structures (bridge-top and top-fcc) have almost identical energies and both structures are experimentally detected on Ni simultaneously.³² We also found that the energy difference between these two structures is 0.003 eV per C atom; thus, we considered both structures as well in a carbon coated model on Ni (Fig. 5a). For comparison, we also considered Ni(111), pristine graphene, and Ni-N₄ embedded graphene (Ni-N₄/Gr), which has been reported as an efficient Ni catalyst for ECR.^{24,25} Based on the XPS results (Fig. 1b), graphitic, pyridinic, and pyrrolic N were considered for investigating the effect of nitrogen content in carbon supports. The optimized structures of reaction models and intermediates are shown in the ESI (Fig. S7–S9†).

The free energy diagrams of electrochemical CO₂ reduction to CO (Fig. 5b) indicate improved catalytic activity of Gr/Ni(111) compared to the other catalysts under comparison here.





Fig. 5 (a) Calculation models for Ni(111) and two graphene structures (bridge-top and fcc-top) for Gr/Ni(111). The free energy diagrams for (b) electrochemical CO₂ reduction to CO and (c) the HER on Ni(111), Gr/Ni(111), pristine graphene and Ni-N₄/Gr.

Pristine graphene shows a high reaction free energy for *COOH formation (2.31 eV), which is the first protonation step for electrochemical CO₂ reduction to CO. Interestingly, Gr/Ni(111) displays a significantly lowered free energy change for *COOH formation (0.58–0.66 eV), even lower than that of Ni-N₄/Gr (1.51 eV) reported previously as an efficient catalyst for the same reaction. Ni(111) shows a lower free energy change for *COOH formation. However, Ni(111) requires a large energy penalty for CO desorption (1.26 eV), indicating overall difficult CO production on the bulk Ni(111) surfaces. In contrast to Ni(111), CO desorption is exothermic on Gr/Ni(111), pristine graphene, and Ni-N₄/Gr. However, it is important to emphasize that, in Gr/Ni(111), Ni(111) plays an important role in improving catalytic activity by greatly stabilizing the *COOH adsorption on graphene but not affecting the easy CO desorption ability of graphene.

In the presence of N in the carbon support, the free energy change for *COOH formation increases in the order of pyrrolic N (−0.71 eV) < pyridinic N (−0.06 eV) < graphitic N (1.34 eV) (Fig. S10†). All of these reaction free energies are lower than that of pristine graphene (2.31 eV), indicating that N can facilitate stabilization of *COOH compared to pristine graphene. The free energy change for CO desorption is also lowered on pyrrolic N (0.79 eV) and graphitic N (−0.79 eV) compared to that of Ni(111) (1.26 eV), except for pyridinic N (1.69 eV). These results suggest that N-doping, particularly in the form of pyrrolic N and graphitic N, can indeed prompt electrochemical CO₂ reduction to CO on the carbon support material, consistent with experiments.

We also found that the hydrogen evolution reaction (HER), which is the most problematic yet dominant side reaction in ECR, can be suppressed on Gr/Ni(111) compared to Ni(111) (Fig. 5c). For the HER, we focused on the strength of H adsorbed on the surface (*H) since that determines the thermodynamic feasibility of the HER and, more importantly, acts as an active site to block ECR.³³ The free energy change for *H formation is highly negative on Ni(111) (−0.41 eV), indicating that *H covers the Ni(111) surface very easily. On the other hand, on

Gr/Ni(111), the free energy change for *H formation is much less favorable (0.10–0.20 eV), meaning that Gr/Ni(111) will be less covered by *H with the active sites made available for ECR.

Conclusions

In summary, we demonstrate that modification of metallic Ni by a combination of carbon coating and incorporation of a N-doped carbon support can effectively suppress the HER and significantly enhance the electroreduction of aqueous CO₂ to CO. This metallic Ni catalyst affords a high CO FE of up to approximately 94% (at −0.7 V vs. RHE) and a current density of 22.7 mA cm^{−2} (at −1.1 V), making it superior to all previous metallic Ni catalysts and even comparable to the best single Ni atom catalysts reported to date. Manipulation of the organic linker type and the addition of carbon black enable tuning of the catalytic properties of the resulting Ni nanoparticles. DFT calculations demonstrate that Ni greatly stabilizes the adsorption of *COOH on Gr/Ni(111) (increased activity) compared to pristine graphene without compromising the easy *CO desorption ability of pristine graphene (selectivity). Also, adding nitrogen-dopants (mainly graphitic N and pyrrolic N configurations) to the carbon support is shown to play an important role in improving catalytic activity by stabilizing *COOH. We believe that this work provides a new scheme to design low cost and active CO₂ reduction catalysts with high selectivity toward CO, which is of importance to both fundamental mechanism studies and technological applications in ECR.

Conflicts of interest

The authors of this manuscript have no conflicts of interest.

Author contributions

M. J., C. M. and H. T. prepared the samples and conducted electrocatalytic tests. M. J., Q. F. and S. L. performed XRD, XPS, FTIR, and SEM characterization experiments. C. C. and Y. J. performed DFT calculations. S. H. performed STEM measurements. T. W. and Y. S. performed EXAFS tests. P. K. and J. Q. helped with discussions on the electrocatalytic results. Z. S. supervised the project and wrote the manuscript. All authors discussed the results and commented on the manuscript.

Acknowledgements

This work was supported by the State Key Laboratory of Organic-Inorganic Composites (No. oic-201503005); the Fundamental Research Funds for the Central Universities (No. buctrc201525); the Beijing National Laboratory for Molecular Sciences (BNLMS20160133); and the State Key Laboratory of Separation Membranes and Membrane Processes (Tianjin Polytechnic University, No. M2-201704). Y. J. acknowledges the support through the National Research Foundation of Korea from the Korean Government (NRF-2017R1A2B3010176).



Notes and references

- Z. L. Wang, C. Li and Y. Yamauchi, *Nano Today*, 2016, **11**, 373–391.
- X. Duan, J. Xu, Z. Wei, J. Ma, S. Guo, S. Wang, H. Liu and S. Dou, *Adv. Mater.*, 2017, **29**, 1701784.
- D. D. Zhu, J. L. Liu and S. Z. Qiao, *Adv. Mater.*, 2016, **28**, 3423–3452.
- A. Vasileff, Y. Zheng and S. Z. Qiao, *Adv. Energy Mater.*, 2017, **7**, 1700759.
- L. Zhang, Z. J. Zhao and J. Gong, *Angew. Chem., Int. Ed.*, 2017, **56**, 11326–11353.
- T. Ma, Q. Fan, H. C. Tao, Z. S. Han, M. W. Jia, Y. N. Gao, W. J. Ma and Z. Y. Sun, *Nanotechnology*, 2017, **28**, 472001.
- Z. Y. Sun, T. Ma, H. C. Tao, Q. Fan and B. X. Han, *Chem*, 2017, **3**, 560–587.
- B. Khezri, A. C. Fisher and M. Pumera, *J. Mater. Chem. A*, 2017, **5**, 8230–8246.
- F. Li, D. R. MacFarlane and J. Zhang, *Nanoscale*, 2018, **10**, 6235–6260.
- D. Voiry, H. S. Shin, K. P. Loh and M. Chhowalla, *Nat. Rev. Chem.*, 2018, **1**, 0105–0122.
- S. Gao, Y. Lin, X. C. Jiao, Y. F. Sun, Q. Q. Luo, W. H. Zhang, D. Li, J. L. Yang and Y. Xie, *Nature*, 2016, **529**, 68–71.
- Y. Jiao, Y. Zheng, P. Chen, M. Jaroniec and S. Z. Qiao, *J. Am. Chem. Soc.*, 2017, **139**, 18093–18100.
- B. Jiang, X. G. Zhang, K. Jiang, D. Y. Wu and W. B. Cai, *J. Am. Chem. Soc.*, 2018, **140**, 2880–2889.
- F. P. Pan, H. G. Zhang, K. X. Liu, D. Cullen, K. More, M. Wang, Z. X. Feng, G. F. Wang, G. Wu and Y. Li, *ACS Catal.*, 2018, **8**, 3116–3122.
- D. F. Gao, H. Zhou, F. Cai, J. Wang, G. Wang and X. H. Bao, *ACS Catal.*, 2018, **8**, 1510–1519.
- T. Zhang, X. Li, Y. Qiu, P. Su, W. Xu, H. Zhong and H. Zhang, *J. Catal.*, 2018, **357**, 154–162.
- S. Zhao, R. X. Jin and R. C. Jin, *ACS Energy Lett.*, 2018, **3**, 452–462.
- H. C. Tao, X. F. Sun, S. Back, Z. S. Han, Q. G. Zhu, A. W. Robertson, T. Ma, Q. Fan, B. X. Han, Y. Jung and Z. Y. Sun, *Chem. Sci.*, 2018, **9**, 483–487.
- Z. S. Han, C. Choi, H. C. Tao, Q. Fan, Y. N. Gao, S. Z. Liu, A. W. Robertson, S. Hong, Y. Jung and Z. Y. Sun, *Catal. Sci. Technol.*, 2018, **8**, 3894–3900.
- Z. Yin, D. F. Gao, S. Y. Yao, B. Zhao, F. Cai, L. L. Lin, P. Tang, P. Zhai, G. X. Wan, D. Ma and X. H. Bao, *Nano Energy*, 2016, **27**, 35–43.
- C. M. Zhao, X. Y. Dai, T. Yao, W. X. Chen, X. Q. Wang, J. Wang, J. Yang, S. Q. Wei, Y. Wu and Y. D. Li, *J. Am. Chem. Soc.*, 2017, **139**, 8078–8081.
- W. Ju, A. Bagger, G. P. Hao, A. S. Varela, I. Sinev, V. Bon, B. R. Cuenya, S. Kaskel, J. Rossmeisl and P. Strasser, *Nat. Commun.*, 2017, **8**, 944–953.
- F. P. Pan, W. Deng, C. Justiniano and Y. Li, *Appl. Catal., B*, 2018, **226**, 463–472.
- H. B. Yang, S. F. Hung, S. Liu, K. Yuan, S. Miao, L. Zhang, X. Huang, H. Y. Wang, W. Cai and R. Chen, *Nat. Energy*, 2018, **3**, 140–147.
- X. G. Li, W. T. Bi, M. L. Chen, Y. X. Sun, H. X. Ju, W. S. Yan, J. F. Zhu, X. J. Wu, W. S. Chu, C. Z. Wu and Y. Xie, *J. Am. Chem. Soc.*, 2017, **139**, 14889–14892.
- Y. Cheng, S. Zhao, B. Johannessen, J. P. Veder, M. Saunders, M. R. Rowles, M. Cheng, C. Liu, M. F. Chisholm and R. De Marco, *Adv. Mater.*, 2018, **30**, 1706287.
- H. C. Tao, C. Yan, A. W. Robertson, Y. N. Gao, J. J. Ding, Y. Q. Zhang, T. Ma and Z. Y. Sun, *Chem. Commun.*, 2017, **53**, 873–876.
- S. Kabir, K. Artyushkova, A. Serov, B. Kiefer and P. Atanassov, *Surf. Interface Anal.*, 2016, **28**, 293–300.
- K. Jiang, S. Siahrostami, A. J. Akey, Y. Li, Z. Lu, J. Lattimer, Y. Hu, C. Stokes, M. Gangishetty and G. Chen, *Chem*, 2017, **3**, 950–960.
- K. Jiang, S. Siahrostami, T. Zheng, Y. Hu, S. Hwang, E. Stavitski, Y. Peng, J. J. Dynes, M. Gangishetty and D. Su, *Energy Environ. Sci.*, 2018, **11**, 893–903.
- Y. Z. Gai, W. C. Wang, D. Xiao and Y. P. Zhao, *Ultrason. Sonochem.*, 2018, **41**, 181–188.
- W. Zhao, S. M. Kozlov, O. Höfert, K. Gotterbarm, M. P. Lorenz, F. Vines, C. Papp, A. Görling and H. P. Steinrück, *J. Phys. Chem. Lett.*, 2011, **2**, 759–764.
- S. M. Sharada, A. R. Singh, B. A. Rohr, Y. Su, L. Qiao and J. K. Nørskov, *Phys. Chem. Chem. Phys.*, 2018, **20**, 4982–4989.

